NeuroImage 124 (2016) 1137–1142

Contents lists available at ScienceDirect

NeuroImage

journal homepage: www.elsevier.com/locate/ynimg

Full Length Article

The Age-ility Project (Phase 1): Structural and functional imaging and electrophysiological data repository

Frini Karayanidis [a,g,h,*], Max C. Keuken [b,f], Aaron Wong [a,g,h], Jaime L. Rennie [a,g,h], Gilles de Hollander [b,f], Patrick S. Cooper [a,g,h], W. Ross Fulham [a,g,h], Rhoshel Lenroot [c], Mark Parsons [d,g,h], Natalie Phillips [e], Patricia T. Michie [a,g,h], Birte U. Forstmann [b,f]

[a] Functional Neuroimaging Laboratory, School of Psychology, University of Newcastle, Australia
[b] Amsterdam Brain and Cognition, University of Amsterdam, 1018 VZ Amsterdam, The Netherlands
[c] Neuroscience Research Australia, University of New South Wales, Australia
[d] School of Medicine and Public Health, University of Newcastle, Australia
[e] Department of Psychology, Concordia University, Canada
[f] Department of Psychology, University of Amsterdam, 1018 VZ Amsterdam, The Netherlands
[g] Priority Research Centre for Translational Neuroscience and Mental Health, University of Newcastle, Australia
[h] Hunter Medical Research Institute, University of Newcastle, Australia

ARTICLE INFO

Article history:
Accepted 21 April 2015
Available online 30 April 2015

ABSTRACT

Our understanding of the complex interplay between structural and functional organisation of brain networks is being advanced by the development of novel multi-modal analyses approaches. The Age-ility Project (Phase 1) data repository offers open access to structural MRI, diffusion MRI, and resting-state fMRI scans, as well as resting-state EEG recorded from the same community participants (n = 131, 15–35 y, 66 male). Raw imaging and electrophysiological data as well as essential demographics are made available via the NITRC website. All data have been reviewed for artifacts using a rigorous quality control protocol and detailed case notes are provided.

Cognitive neuroscience focuses on understanding the functional and structural organisation of brain networks and how they support cognition. This work has been enabled by the emergence of multiple brain imaging modalities that take advantage of different physical properties of brain tissue. For instance, diffusion MRI (dMRI), which relies on the diffusion property of water molecules, has provided unprecedented insight into the structural organisation of white matter and its malleability to both development and experience. Likewise, by taking advantage of the properties of the brain's hemodynamic response, functional MRI (fMRI) quantifies differential activation in distinct brain regions at task vs. baseline. While each brain imaging modality is making a valuable contribution to the construction of the bigger picture, they all come with their own aperture limitations. The complete picture is therefore likely to emerge from the development of novel analysis approaches that will bring together knowledge across different imaging modalities.

The present data repository aims to contribute to this objective by offering access to structural and functional imaging data, as well electrophysiological data recorded from 131 participants aged 15–35 years. This dataset can be used to probe a range of questions regarding the relationship between functional and structural properties of brain signals derived from different approaches. For instance, as EEG and MRI were acquired from the same participants, these data may be useful in developing multi-model methods.[1]

The Age-ility project

The Age-ility Project Phase 1 investigates the relationship between cognitive control and the presentation of adaptive and maladaptive behaviours across the adult lifespan. The primary research question is whether individual differences in cognitive flexibility and maturation of associated brain pathways can explain variability in propensity towards risk-taking behaviours and maladaptive outcomes in young adults. Data collection for Phase 1 was completed in December 2014 and includes a comprehensive assessment of cognitive functioning and brain structure and function in a community sample of young

* Corresponding author at: Functional Neuroimaging Laboratory, School of Psychology, University of Newcastle, NSW 2308, Australia.
E-mail address: Frini.Karayanidis@newcastle.edu.au (F. Karayanidis).

[1] It is beyond the scope of the current manuscript to go in-depth about the methodological challenges associated with this multimodal integration. The interested reader is referred to papers that discuss combining MRI and EEG data (e.g., Halchenko et al., 2005, Lamm et al., 2000, Schwartz et al., 1996, Spiclin et al., 2007).

http://dx.doi.org/10.1016/j.neuroimage.2015.04.047
1053-8119/

people aged 15–35 years. This community sample of 237 participants completed a comprehensive neuropsychological and psychometric assessment, including subtests of the Wechsler Abbreviated Scale of Intelligence—2nd Edition (WASI-II, Wechsler, 1999), the Cambridge Neuropsychological Test Automated Battery (CANTAB, Cambridge Cognition Limited, www.cambridgecognition.com), and the Achenbach System of Empirically Based Assessment (ASEBA, www.aseba.org/, Achenbach, 2009), as well as other psychometric scales. In addition, an electroencephalogram (EEG) was recorded both at rest and while participants performed a task-switching paradigm (Karayanidis et al., 2009) and a stop-signal task (Forstmann et al., 2012). Ongoing data collection includes longitudinal testing of this sample at 2 y and 4 y (Phases 2 and 3, respectively), extension of the age range to cover the adult lifespan (up to 80y) and clinical groups that show compromised cognitive control.

The Age-ility Project Phase 1 data on the Neuroimaging Informatics Tools and Resources Clearinghouse (NITRC) website include all the imaging data collected as part of this protocol. One hundred and thirty seven participants aged 15–35 y who met inclusion criteria for brain imaging completed a magnetic resonance imaging (MRI) session that included a structural MRI, two diffusion MRI sequences and a resting-state functional MRI sequence, as well as resting-state EEG and essential demographic information. Data from six participants were excluded: two had a clinical finding (i.e., pineal cyst) and four were missing rs-fMRI scans.

All imaging files have undergone intensive quality control and de-identification, using procedures described below. These quality-controlled, de-identified raw data files in universally accessible format and minimal demographic information (age, sex) are made available on the NITRC website (http://www.nitrc.org/projects/age-ility/). Data from neuropsychological, psychometric and cognitive tasks are not currently being made available as publications pertaining to the main research questions of the Age-ility Project are still ongoing. However, the full testing protocol is available for review (AgeilityProject(Phase1)FullProtocol.pdf in http://www.nitrc.org/projects/age-ility/) and specific demographic, neuropsychological and psychometric information may be made available to individual projects, upon request. Following the Phase 1 publication cycle, this information will be linked to the database on NITRC. In addition, Phase 2 and Phase 3 data will be made available when data collection for these phases is complete.

Data parameters and quality control

The Age-ility Project (Phase 1) data repository includes imaging data from participants recruited from a range of community sources, including high schools, professional training colleges, university and community groups. Equivalent numbers of males and females were recruited with similar age and handedness scores (Table 1). A brief telephone screening interview was used to exclude participants who reported current or past diagnosis of psychiatric illness, neurological condition or head trauma, or who failed to meet criteria for MRI (e.g., claustrophobia, pregnancy, metal implants). A large number of young people were also excluded from imaging because they had dental braces or permanent dental wires that produced excessive artifact in the MRI signal (Klinke et al., 2012). Participants were asked to abstain from caffeine and alcohol at least 2 h prior to each of three testing sessions. The first session included comprehensive neuropsychological and psychometric testing. The second session included EEG recording at rest and during task-switching and stop-signal paradigms. The third session included the brain imaging protocol. The Age-ility protocol was approved by the University of Newcastle Human Research Ethics Committee (HREC: H-2012-0157). All participants gave written informed consent, and parental consent was also acquired for participants under 18 y of age. Financial reimbursement of $20/h was offered, with a maximum of $200/participant.

Table 1
Sample characteristics. Mean score (and standard deviation) for age and days between sessions.

	Male	Female	Total
n	66	65	131
Age (yrs)	20.80 (*4.62*)	22.65 (*5.71*)	21.72 (*5.25*)
Right-handed (n)	58	58	116
Days b/w sessions:			
S1 v S2	12.95 (*12.46*)	12.48 (*11.14*)	12.72 (*11.78*)
S2 v S3	31.48 (*34.15*)	42.82 (*39.41*)	37.11 (*37.15*)

The data descriptor file shows the participant code that links all files, as well as age, sex, handedness and days between sessions for each individual (DataDescriptorFile.xlsx in http://www.nitrc.org/projects/age-ility/; see also Supplement 1 (Supplement1_DataDescriptorFile.xlsx)). Handedness was determined based on the hand that participants reported using to write and throw a ball, *and* they identified as dominant when completing the Grooved Pegboard Test (Lafayette Instrument Co). One participant did not consistently identify the same hand above and is marked as 'query right-handed'. The data descriptor file also contains notes related to the quality of the raw MRI and EEG data based on procedures described below.

MRI data

All MRI data were acquired on the Siemens Skyra 3 T whole-body scanner equipped with a 32-channel headcoil at the Calvary Mater Hospital, Newcastle, Australia. A fixed order acquisition session was run by a clinically registered radiographer and an experimenter. The session lasted a total of approximately 55–65 min and included T1, DWI B3000, DWI B1000, and resting-state fMRI sequences run in that order. In a few participants, the DWI B3000 sequence failed and was repeated at the end of the scanning session. The order that successful sequences were acquired is also listed in the data descriptor file. A vitamin pill was placed on the participant's right temple and shows as a hyperintense ball outside of the skull on the T1-weighted MPRAGE scans. Participants listened to music through earbud earphones for all sequences, except the rs-fMRI sequence (Fig. 1).

In order to de-identify data, all information that could identify any individual, including study-specific participant codes, was removed using an automated procedure. Participants were given a sequential integer ID that reflects the recruitment order. DICOM MR images were converted to NIFTI format using 'dcm2nii' that is part of the software package mricron:(www.mccauslandcenter.sc.edu/mricro/mricron/dcm2nii.html).

T1 sequence

The T1 protocol used a T1-weighted MPRAGE protocol (Mugler and Brookeman, 1990; TR = 2200 ms, TE = 3.5 ms, flip angle = 7°, 256 × 256 matrix, FoV = 256 mm, voxel size 1 mm isotropic, 176 slices, GRAPPA = 2, Bandwidth = 190 Hz/Px, duration 6.45 min). See Supplement 2 (Supplement2_MPRAGE_exam_card.xlsx) for the T1-weighted MPRAGE MRI exam card.

These files were rated for artifacts and then de-identified using an automatic de-facing workflow that masks the voxels around the nose (Bischoff-Grethe et al., 2007). This output was once again reviewed to ensure that face was correctly removed and that the brain remained intact. To ensure that the de-faced masks did not remove parts of the brain in the other sequences, the masks were eroded with a 3 × 3 × 3 Gaussian kernel. For five cases, the de-facing result eroded parts of the brain. For those cases, we manually created a de-face mask for each case and applied it to the T1 scan.

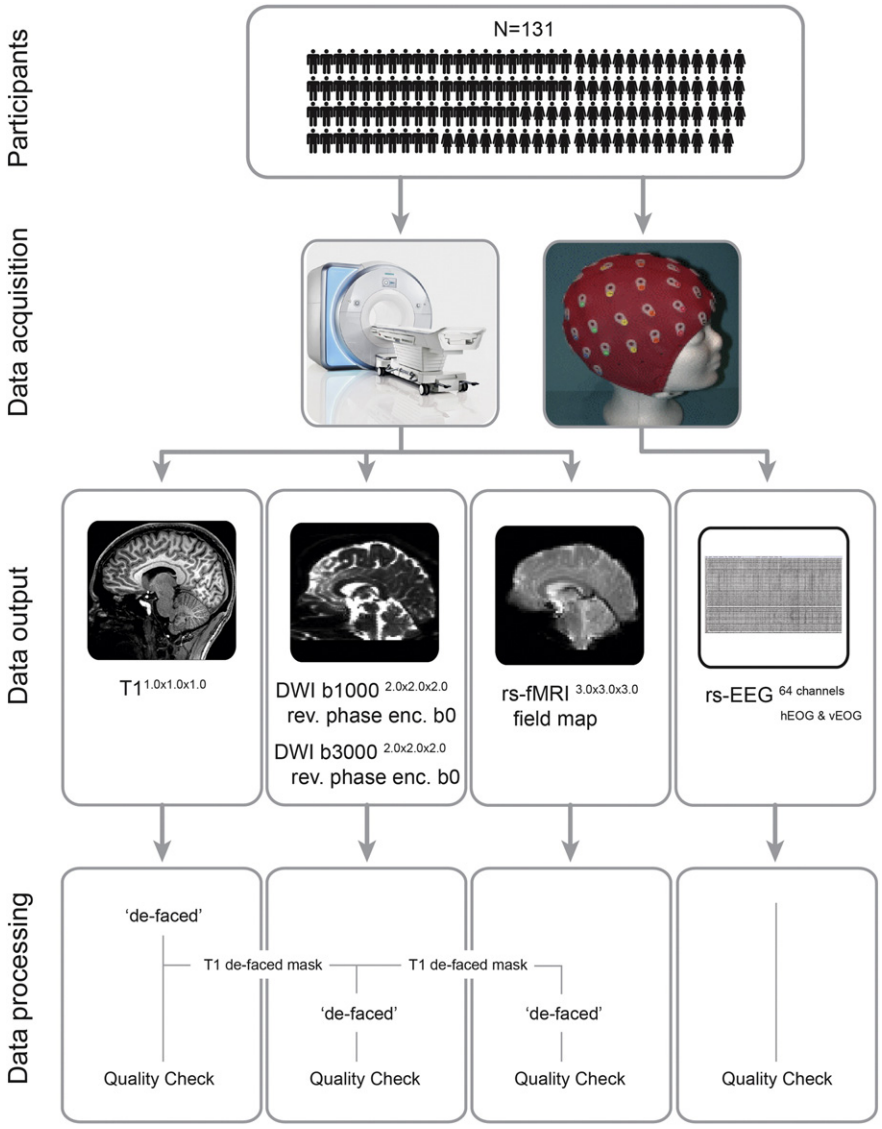

Fig. 1. Data acquisition procedure. Neuroimage data were collected from 131 young participants aged of 15 and 35 years. Data acquisition included a structural T1-weighted MRI scan, two diffusion weighted MRI scans, and a resting-state functional MRI scan using a 3 T MRI scanner. Additionally, resting-state EEG from 64 channels was acquired. All data were anonymised and checked for artifacts. See text for details.

Diffusion MRI

Two acquisitions were performed using an optimised version of the Siemens diffusion tensor sequence. The first acquisition included a diffusion weighting of b = 3000 s/mm^2 (TR = 15,300, TE = 108 ms, FoV = 240 mm, 120 × 120 matrix, voxel size 2 mm isotropic, 70 slices). The second acquisition included a diffusion weighting of b = 1000 s/mm^2 (TR = 11,000 ms, TE = 108 ms, FoV = 240 mm, 120 × 120 matrix, voxel size 2 mm isotropic, 70 slices). For both acquisitions, diffusion weighting was isotropically distributed along 64 directions, with an additional volume with no diffusion weighting (b0) obtained at the start of each acquisition. A pair of reverse phase encoded b0 images were also acquired before each DWI scan to account for susceptibility-induced distortion (Duration: B1000 = 46 s each; B3000 = 1:03 min each) (Andersson et al., 2003; Smith et al., 2004). See Supplement 3 (Supplement3_DWI_exam_card.xlsx) for the Diffusion weighted MRI exam card.

The T1 defacing mask from each participant was used to de-identify the diffusion MRI images. The T1 image was registered to the b0 volume using the default settings in flirt, which is part of the FSL software package (5.0.6). The defacing mask was then transformed to DWI space using the resulting transformation matrix. The registered defacing mask was used to anonymise the diffusion MRI volume. This was done for both the B1000 and B3000 volumes. Subsequently, all volumes were manually checked to ensure that the de-face mask did not remove any parts of the brain. If this occurred the masks were manually adjusted in DWI space and reapplied.

Resting state fMRI

Images were acquired using a T2*-weighted echo planar imaging sequence (EPI, Mansfield, 1977; 3 mm slice thickness, 60 slices, TR = 3120 ms, TE = 21 ms, flip angle = 90°, FOV = 288 mm, 96 × 96 matrix, voxel size = 3 × 3 × 3 mm, 160 scans per run). EPIs were obtained as interleaved axial slices (without gap) tilted −3° to the true axial plane in scanner coordinates. A gradient-echo field map was also acquired for subsequent susceptibility-induced distortion correction (3 mm slice thickness, 60 slices, TR = 500 ms, TE = 3.48 ms, flip angle = 55°, FoV = 288 mm, 96 × 96 matrix, voxel size 3 mm isotropic, GRAPPA = 2, bandwidth = 1796 Hz/Px). In addition a field map was acquired to account for susceptibility-induced distortion (duration 1:39 min). Participants were instructed to keep their eyes closed but avoid

sleeping (Duration 8.32 min). See Supplement 4 (Supplement4_rs-fMRI_exam_card.xlsx) for the T2*-weighted EPI MRI exam card.

The T1 defacing mask from each participant was also used to de-identify the rs-fMRI files using a similar method as for the DWI volumes. To improve the T1 registration to the rs-fMRI space, a mean rs-fMRI volume was created. The rs-fMRI file was first motion corrected using mcflirt and a mean rs-fMRI volume was calculated using fslmaths. The T1 volume was registered to the mean rs-fMRI volume. The defacing mask was transformed to the rs-fMRI space using the resulting transformation matrix. The registered defacing mask was then applied to anonymise the original rs-fMRI volume. All volumes were manually checked to ensure that the de-face mask did not remove any parts of the brain. If this occurred, the masks were manually adjusted in the original rs-fMRI space and reapplied.

Artifact quality control motion

For the T1 weighted MPRAGE volume, motion artifacts were estimated by calculating the noise ratio between the phase encoding direction and the read direction outside of the brain (Forstmann et al., 2014; Gedamu et al., 2008). Two ROIs of 400 mm^2 were manually defined in the coronal and axial plane. The mean standard deviation was extracted from both ROIs and the phase encoding direction signal was divided by the read direction signal. Low ratio scores indicate low motion artifact, and a ratio below 2 reflects little to no motion artifact present (Gedamu et al., 2008). The mean ratio was 1.59 (sd 0.72).

For the DWI and rs-fMRI volumes, the amount of motion was estimated using mcflirt, which is part of the FSL software package (Jenkinson et al., 2002). This outputs two general motion indices: absolute mean displacement, which is the average displacement relative to the middle volume, and relative mean displacement, which is the average displacement from volume to volume.

We examined whether overall motion artifact and type of motion artifact differed between imaging sequences using a repeated measures ANOVA [3 sequence type (B1000, B3000, rs-fMRI data) × 2 motion type (absolute, relative mean displacement)]. There were significant main effects of sequence type ($F(2,129) = 723.7$, $p < 0.001$) and motion type ($F(1,130) = 403.3$, $p < 0.001$) (Fig. 1). Post-hoc testing using Bonferroni correction showed that the B3000 volumes contained more absolute motion than the B1000 ($t(130) = 19.43$, $p < 0.001$) which, in turn, contained more absolute motion than the rs-fMRI volumes ($t(130) = 13.39$, $p < 0.001$). A similar pattern of differences was found for the relative motion measure (B1000 vs. B3000: $t(130) = 26.86$, $p < 0.001$; B1000 vs. rs-fMRI: $t(130) = 34.13$, $p < 0.001$) (Fig. 2).

The difference in motion may be, at least partly, due to differences in the acquisition length of the sequence. This is consistent with the fact that motion effects reduced with decreasing acquisition length (i.e., B3000 > B1000 > rs-fMRI). However, it is also possible that eddy currents may result in motion-like image distortions in the high b-value DWI dataset (Chan et al., 2014). See Ben-Amitay et al. (2011) for a preprocessing pipeline that is specific for high b-value DWI data.

Spiking

For the rs-fMRI volumes, the data were checked for intensity and motion outliers across volumes that were greater than two standard deviations from the mean, using the rapidart NIPY pipeline (Gorgolewski et al., 2011). This allowed the identification of spikes, which might reflect electrical sparks, rapid motion, or external interference. On average, 8.07 (std 4.26) of a total of 160 volumes were classified as containing an artifact.

Signal to noise ratio

The signal to noise ratio (SNR) in the T1 weighted MPRAGE volume was estimated by dividing the mean brain tissue signal from an axial slice just above the corpus callosum by the standard deviation of the signal in the read direction ROI. For DWI volumes, SNR was calculated on the B0 images. For rs-fMRI, it was based on the mean rs-fMRI volume. To improve the estimation of noise, a Rician correction was applied (Gudbjartsson and Patz, 1995). We use the term SNR_{approx} to indicate that this is still an approximation of SNR. Mean SNR_{approx} for T1 was 186.88 (std. 91.75), for b3000 B0 volume was 29.37 (std. 8.82), for B1000 B0 volume was 72.79 (std. 22.18), and for the mean rs-fMRI was 426.33 (std. 109.82). In addition to mean SNR of the rs-fMRI, temporal SNR was also calculated using the tSNR pipeline implemented in nipype (http://nipy.sourceforge.net/nipype/interfaces/generated/nipype.algorithms.misc.html#tsnr). The mean tSNR for the rs-fMRI was 61.08 (std. 11.88). Participants who scored more than 2 standard deviations from the group mean on either SNR measure are noted in the data descriptor file with an asterisk.

Visual inspection

All MRI volumes were also manually checked by one trained assessor for ghosting, wrapping, inhomogeneous shading, spiking and Moire fringes ("zebra stripes"). The DWI and rs-fMRI volumes were also checked for severe susceptibility artifacts and temporal spikes. Ghosting artifacts are generally caused by motion and appear as a 'ghost' image of the brain in the phase encoding direction. Wrapping artifacts are usually caused by anatomical features protruding outside of the imaged field of view but still within the sensitive volume of the RF coil. Shading artifacts were defined as non-homogenous intensity throughout the entire brain. Moire fringes were defined as well-defined alternating black and white stripes across the brain. Temporal spikes were defined as unexpected large changes of overall intensity in the volume over gradients or time (Forstmann et al., 2014; McRobbie et al., 2006).

A score was given for each of the above artifacts, using the following scale: 1: absent, 2: present but does not overlap with brain areas, 3: present but minor, 4: present and severe. The rating for each scale for each checked volume is listed in Supplement 1 (Supplement1_DataDescriptorFile.xlsx).

EEG data

EEG was recorded continuously using an ActiveTwo Biosemi EEG system (2048 Hz, bandpass filter of DC-400 Hz) from 64 scalp electrodes plus bilateral mastoids and ocular sites (outer canthi, supraorbital, infraorbital), arranged according to the Modified Combinatorial Nomenclature (MCN). Biosemi ActiveTwo systems utilise active electrodes and so high impedances can be better tolerated. Data are recorded so that no outlying electrode offsets are present, rather than keeping impedance below a threshold. Common mode sense (CMS) and driven right leg (DRL) electrodes were positioned inferior to P1 and P2, respectively. EEG data were recorded relative to an amplifier reference voltage, and then re-referenced in software to the Cz electrode to remove common-mode signals. Three 2 min intervals of resting-state EEG were acquired before, half-way through and immediately after the completion of a task-switching paradigm. Participants were instructed to keep still with their eyes closed. An instruction screen was presented to the participant, informing them to close their eyes. This screen lasted for 30 s, after which a blank screen appeared to mark the start of the resting period. Its onset was marked in the continuous EEG file by an event marker.

The three epochs of resting-state EEG were extracted from the continuous EEG file and saved as separate European Data Format (.edf) files for each participant. Each epoch was 3 min including 2 min of resting-stage EEG and 30 s baselines before and after the resting-state period. The entire 30 second pre- and post-rest baseline was not always available for the first and third resting-state interval respectively. These cases are noted in the data descriptor file and these affected periods were zero-padded to ensure 3 min of data are available.

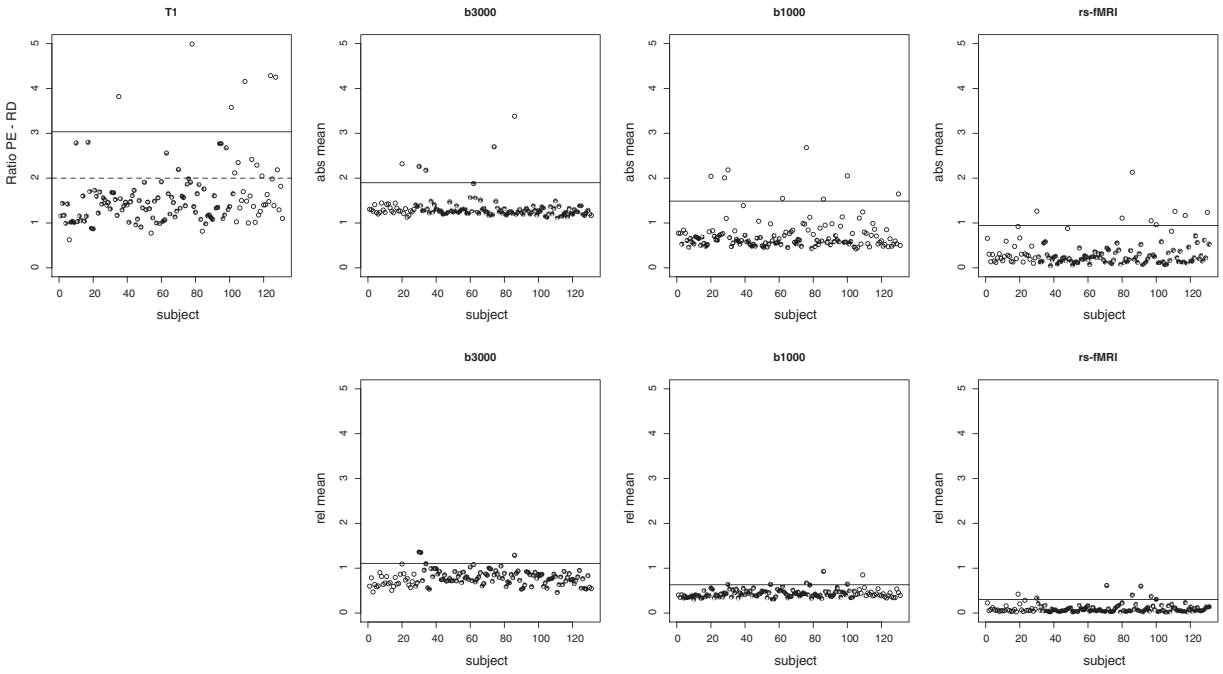

Fig. 2. Motion estimates for each imaging sequence. The first column shows the noise ratio between the phase encoding direction and the read direction outside of the brain for the T1 weighted MPRAGE sequence. The remaining columns show the absolute mean displacement and relative mean displacement per sequence as calculated by mcflirt. The solid line indicates two standard deviations from the mean; the dotted line indicates the proposed cut-off point by Gedamu et al. (2008). See text for details.

Artifact quality control

Each epoch of raw resting EEG data was inspected for artifact using a semi-automated process which included visual inspection by a trained assessor and signal-to-noise ratio (EEG-SNR) thresholding. Artifact included high frequency period noise (i.e., 50 Hz line noise), gross muscle artifact and low frequency drift. EEG-SNR was computed as mean(C_i) / mean(ε), where C_i is i-th recorded channel of the electrode montage filtered with a 1 Hz high-pass Butterworth filter and ε is the noise. Noise was defined as the difference between predicted signal of C_i (via interpolation of surrounding electrode sites with the same filter settings as before) and C_i. An EEG-SNR of less than 1.5 was used to classify channels as noisy. EEG data are unprocessed and hence epochs with artifact are likely to be useful after typical data cleaning preprocessing steps are applied. Atypical artifacts were also identified (e.g., poor electrode contact) but occurred less frequently than typical artifacts defined above. Channels with artifact for each participant are listed in Supplement 1 (Supplement1_DataDescriptorFile.xlsx). While most participants are listed as having at least one noisy channel in the unprocessed EEG data, many of these electrodes will be useful after typical data preprocessing. Average SNR for EEG are in shown in Fig. 3. For cases without resting state epochs, the SNR is denoted as 0.

Access to data

Data are available on the open access NITRC site (https://www.nitrc.org/projects/age-ility/) as well as a server at the University of Newcastle (http://hdl.handle.net/1959.13/1061314). Institutional ethics approval has been obtained to make these de-identified data openly available, so there are no limitations for access. However, in order to be able to inform users of any changes to the status of the data (e.g., retraction or addition of cases, addition of measures), we will seek minimal information from prospective users (name, institution, email). To access to any other measures (e.g., additional demographic information or scores from neuropsychological, psychometric and/or cognitive tasks), prospective users will be required to contact us directly. Links to such information will be supplied through our institutional server after obtaining institutional ethics approval.

Resource management and contribution of new data

NITRC is sponsored by the National Institutes of Health Blueprint for Neuroscience Research. The corresponding author will be responsible for authorising any change in data available and addition of new information on both the NITRC and the University of Newcastle site. Data

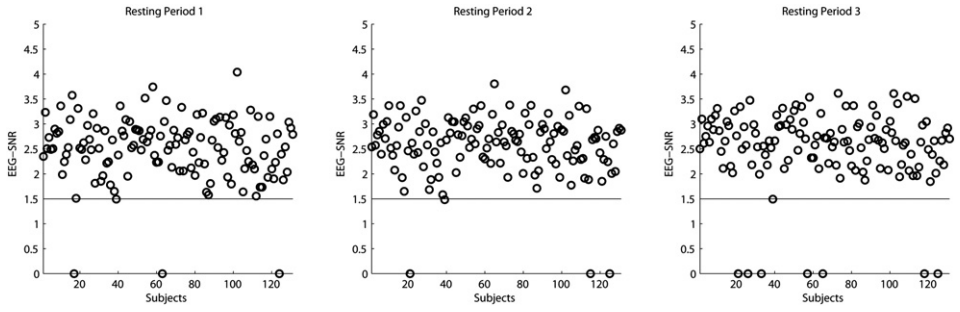

Fig. 3. Average EEG-SNR for each participant in each of the three resting EEG periods. An EEG-SNR of less than 1.5 was used to classify channels as noisy and is shown as the solid line. Missing epochs are denoted with an SNR value of 0. See text for details.

from Phase 2 and Phase 3 of the Age-ility Project will be made available at a later date. Given that all the data were collected from the same scanner and EEG system, datasets from other facilities cannot be added without changing the consistency of the dataset.

Acknowledgments

This work was supported by an Australian Research Council Discovery Project grant (ARC-DP 120100340) to Karayanidis, Forstmann, Michie, Parsons, Wagenmakers, Phillips, Lenroot. Cooper and Rennie were supported by an Australian Postgraduate Award. This research line is financially supported by the European Research Council (BUF) (ERC-2012-StG-313481). We thank Jameen Arms, head radiographer at the Calvary Mater Hospital, for his team's support with imaging, Tony Kemp and Gavin Cooper for technical support, and Elise Mansfield, Renate Thienel, Vanessa Case, Paul Garrett, Natalie Lantry, Olivia Whalen, Samantha Allen, Montana Hunter, Laura Williamson, Courtney Phillips, Cathryn Mackenzie and Patrick Skippen for their contribution to recruitment, data collection, data entry and quality control.

Appendix A. Supplementary data

Supplementary data to this article can be found online at http://dx.doi.org/10.1016/j.neuroimage.2015.04.047.

References

Achenbach, T.M., 2009. The Achenbach System of Empirically Based Assessments (ASEBA): Development, Findings, Theory, and Applications. University of Vermont Research Center for Children, Youth, & Families, Burlington, VT.

Andersson, J.L.R., Skare, S., Ashburner, J., 2003. How to correct susceptibility distortions in spin-echo echo-planar images: application to diffusion tensor imaging. NeuroImage 20 (2), 870–888. http://dx.doi.org/10.1016/S1053-8119(03)00336-7.

Ben-Amitay, S., Jones, D.K., Assaf, Y., 2011. Motion correction and registration of high b-value diffusion weighted images. Magn. Reson. Med. 67 (6), 1694–1702. http://dx.doi.org/10.1002/mrm.23186.

Bischoff-Grethe, 2007. A technique for deidentification of structural brain MR Images. Hum. Brain Mapp. 28, 892–903.

Chan, R.W., Deuster, von, C., Giese, D., Stoeck, C.T., Harmer, J., Aitken, A.P., et al., 2014. Journal of magnetic resonance. J. Magn. Reson. 244 (C), 74–84. http://dx.doi.org/10.1016/j.jmr.2014.04.018.

Forstmann, B.U., Keuken, M.C., Jahfari, S., Bazin, P.L., Neumann, N., Schafer, A., et al., 2012. Cortico-subthalamic white matter tract strength predict interindividual efficacy in stopping a motor response. NeuroImage 60, 370–375.

Forstmann, B.U., Keuken, M.C., Schäfer, A., Bazin, P.-L., Alkemade, A., Turner, R., 2014. Multi-modal ultra-high resolution structural 7-Tesla MRI data repository. Sci. Data 140050 http://dx.doi.org/10.1038/sdata.2014.50 (1 SP - EP -).

Gedamu, E.L., Collins, D.L., Arnold, D.L., 2008. Automated quality control of brain MR images. J. Magn. Reson. Imaging 28, 308–319.

Gorgolewski, K., Burns, C.D., Madison, C., Clark, D., Halchenko, Y.O., Waskom, M.L., Ghosh, S.S., 2011. Nipype: a flexible, lightweight and extensible neuroimaging data processing framework in Python. Front. Neuroimform. 5, 13.

Gudbjartsson, H., Patz, S., 1995. The Rician distribution of noisy MRI data. Magn. Reson. Med. 34, 910–914.

Halchenko, Y.O., Hanson, S.J., Pearlmutter, B.A., 2005. Multimodal Integration: fMRI, MRI, EEG, MEG. In: Landini, L., Positano, V., Santarelli, M.F. (Eds.), *Advanced imaging processing in magnetic resonance imaging*.Dekker, pp. 223–265

Jenkinson, M., Bannister, P., Brady, J.M., Smith, S.M., 2002. Improved optimisation for the robust and accurate linear registration and motion correction of brain images. NeuroImage 17 (2), 825–841.

Karayanidis, F., Mansfield, E., Galloway, K., Smith, J., Provost, A., Heathcote, A., 2009. Anticipatory reconfiguration elicited by fully and partially informative cues that validly predict a switch in task. Cogn. Affect. Behav. Neurosci. 9, 202–215. http://dx.doi.org/10.3758/CABN.9.2.202.

Klinke, T., Daboul, A., Maron, J., Gredes, T., Puls, R., Jaghsi, A., Biffar, R., 2012. Artifacts in magnetic resonance imaging and computed tomography caused by dental materials. PLoS ONE 7 (2), e31766. http://dx.doi.org/10.1371/journal.pone.0031766.t005.

Lamm, C., Windischberger, C., Leodolter, U., Moser, E., Bauer, H., 2000. Co-registration of EEG and MRI data using matching of spline interpolated and MRI-segmented reconstructions of the scalp surface. Brain Topography 14 (2), 93–100. http://dx.doi.org/10.1023/A:1012988728672.

Mansfield, P., 1997. Multi-planar image formation using NMR spin echoes. J. Phys. C 10, L55–L58.

McRobbie, D.W., Moore, E.A., Graves, M.J., Prince, M.R., 2006. MRI from Picture to Proton. 1st ed. Cambridge University Press, Cambridge.

Mugler, J.P., Brookeman, J.R., 1990. Three-dimensional magnetization-prepared rapid gradient-echo imaging (3D MP RAGE). Magn. Reson. Med. 15, 152–157.

Schwartz, D., Lemoine, D., Poiseau, E., Barillot, C., 1996. Registration of MEG/EEG data with 3D MRI: Methodology and precision issues. Brain Topography 9 (2), 101–116.

Smith, S.M., Jenkinson, M., Woolrich, M.W., Beckmann, C.F., Behrens, T.E.J., Johansen-Berg, H., et al., 2004. Advances in functional and structural MR image analysis and implementation as FSL. NeuroImage 23, S208–S219. http://dx.doi.org/10.1016/j.neuroimage.2004.07.051.

Spiclin, Z., Hans, A., Duffy, F.H., Warfield, S.K., Likar, B., Pernus, F., 2007. EEG to MRI registration based on global and local similarities of MRI intensity distributions. Audio and Electroacoustics Newsletter, IEEE 11 (Pt 1), 762–770.

Wechsler, D., 1999. Wechsler Abbreviated Scale of Intelligence. The Psychological Corporation, San Antonio, TX.